

Supplementary material E. d'Ambrosio, F. Blanc, E. Lemaire
Université Côte d'Azur, CNRS, InPhyNi-UMR 7010, 06108 Nice Cedex 2,
France

Supplementary material of "Viscous resuspension of non-Brownian particles: determination of the concentration profiles and particle normal stresses".

Enzo d'Ambrosio¹, Frédéric Blanc¹
Elisabeth Lemaire¹elisabeth.lemaire@unice.fr

November 26, 2020

1 Particle size distribution

Particle size distribution is determined from image analysis and is shown in Figure 1.

2 Particle distribution and velocity fields for all the angular velocities

The (r, z) concentration, azimuthal and vertical velocity fields for the all set of experiments are shown in figure 2.

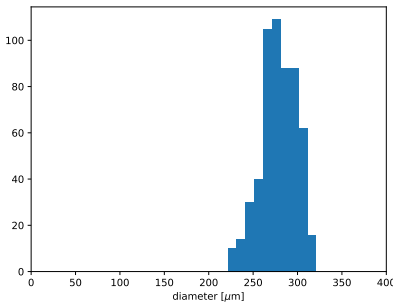


Figure 1: Particle size distribution obtained from image analysis.

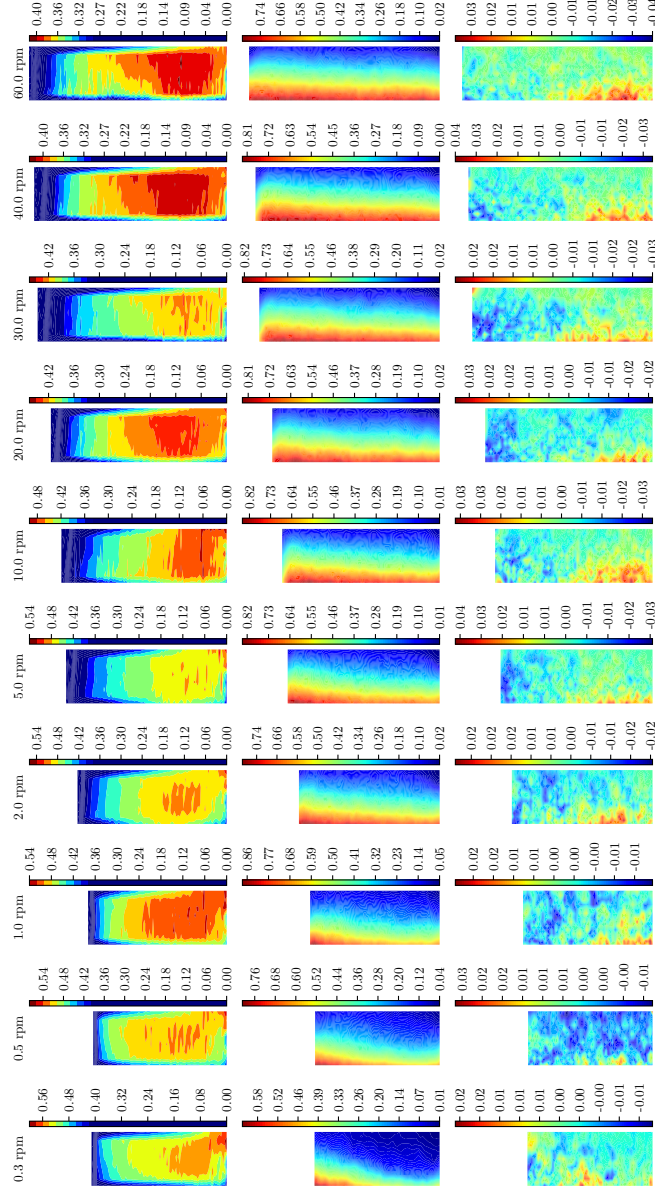


Figure 2: 2D fields for all the sets of experiments. First line: mapping of the particle volume fraction averaged over 10000 images. Second line: azimuthal velocity normalized by the rotor velocity ΩR_1 and averaged over 100 velocity fields. Third line: vertical velocity normalized by ΩR_1 and averaged over 100 velocity fields. The rotor is on the left of each frame, the stator is on the right, and the mercury/suspension interface corresponds to the bottom of each frame.

3 Velocity profiles for a shear-thinning material

For a shear-thinning constitutive law given by $\Sigma_{12} \propto \dot{\gamma}^n$, the velocity profile is :

$$v_{\theta}/\Omega R_i = \frac{(R_e/r)^{2/n-1} - r/R_e}{(R_e/R_i)^{2/n-1} - R_i/R_e} \quad (1)$$

Figure 3 shows the radial velocity profiles that correspond to the concentration profiles of figure 3 of the main paper ($v(r)$ -profiles z-averaged over one tenth of the resuspended layer height for $\Omega = 0.3$ and 20 rpm). In figure 3 are also plotted some theoretical velocity profiles. The solid lines correspond to Newtonian profiles, the dashed line to Newtonian profiles with wall slip, the dotted lines to shear-thinning profiles (1) computed with the exponent $n = 0.7$ found in section 3.3.2 and equation (3.3) of the main paper.

4 On possible size segregation

As discussed in the main article, the radial concentration profiles do not obey the SBM predictions and we sought to understand the reasons for this discrepancy. One of the possible cause that we have examined is the size segregation since the particles are not perfectly monodisperse. The larger particles are expected to migrate faster than the smaller ones and then to be focused at the outside while the smaller are preferentially located near the rotor. Since, in our study, the particle volume fraction is deduced from the particle number density, a size gradient across the gap could possibly affect the concentration profiles. To determine if there is or not size segregation, we first measure the apparent radius of the particles across the gap. Figure 4 shows the apparent radius of the particles as a function of their radial position in the gap. No significant size gradient is observed. The close examination of the figure 3 of the main paper, however, indicates that, in the layered zones the inter-band distance is slightly larger at the stator than at the rotor. We wondered if it was or not a hint of size segregation (with the larger particles leading to thicker bands near the stator) and if, indeed, the band spacing was an indicator of the particle size. To answer this question, we extracted from our experiments the inter-band distance *at the rotor* and plotted it against the local shear rate for several volume fractions ($\phi = 0.41 \pm 0.01$, 0.46 ± 0.01 and 0.51 ± 0.01). The results are presented in the figure 5 and show that the inter-band distance varies with particle volume fraction (as already shown by numerical simulation by [Yeo & Maxey(2010)] or by [Gallier *et al.*(2016)Gallier, Lemaire, Lobry & Peters]) and also with shear rate: the inter-band distance decreases with both particle volume fraction and shear rate. Thus, since the shear rate is lower at the stator than at the rotor, it is expected that, if the particle volume fraction is constant across the gap, the inter-band distance is smaller at the rotor than at the stator. On the opposite, in the case of a neutrally buoyant suspension, where radial particle migration is clearly measured see figure 13 of the main manuscript), the competing effects of the outward gradient of particle volume fraction and the inward gradient of

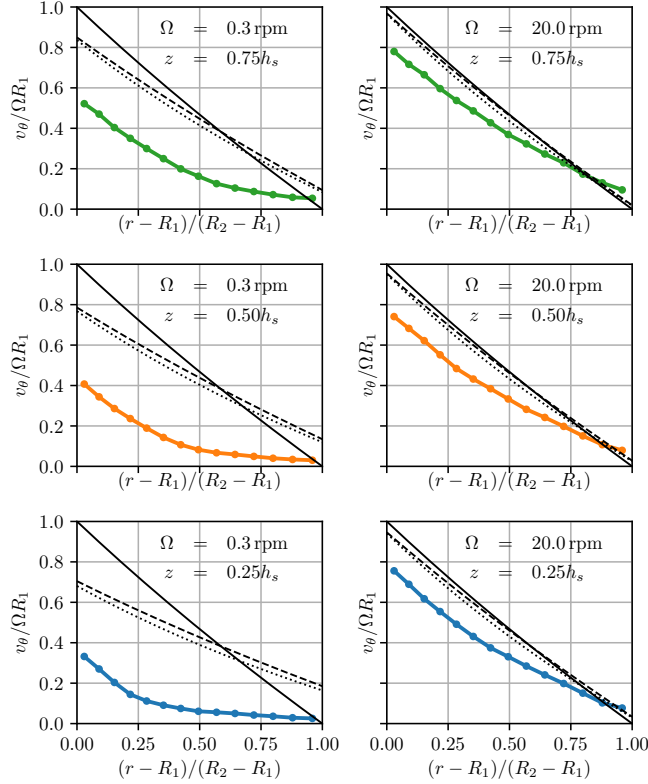


Figure 3: Azimuthal velocity profiles measured for angular velocities: $\Omega = 0.3 \text{ rpm}$ and 20 rpm at three different heights: $h_s/4$, $h_s/2$ and $3h_s/4$. Are also shown the theoretical profiles corresponding to the mean particle volume fraction measured at the corresponding heights. Solid lines: Newtonian profiles without wall slip, dashed lines: Newtonian profiles with wall slip evaluated from [Jana *et al.*(1995)Jana, Kapoor & Acrivos], dotted lines: shear-thinning profiles (1) computed with $n = 0.7$ and wall slip evaluated from [Jana *et al.*(1995)Jana, Kapoor & Acrivos].

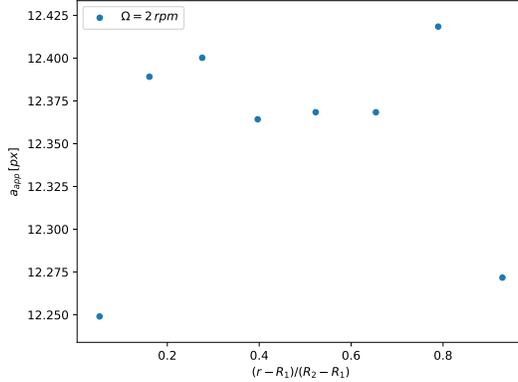


Figure 4: Apparent radius of the particles as a function of their radial position in the gap

shear rate may contingently lead to roughly equal inter-band distances at the stator and at the rotor as observed in the figure 13 of the main paper.

Thus, as a conclusion, we did not find any evidence of size segregation which consequently cannot explain the discrepancy observed between the measured concentration profiles and the SBM predictions.

5 Evaluation of the influence of the 2D character of the flow

The velocity profiles shown in figure 2 of the main paper display indisputable 2D characteristics of the flow for the lowest angular velocities. Our purpose here is to evaluate the error which is introduced when a 1D flow approximation is used.

The rate of strain tensor is given by

$$e_{ij} = \left(\frac{\partial u_i}{\partial x_j} + \frac{\partial u_j}{\partial x_i} \right) \quad (2)$$

We now evaluate all the components of e_{ij} .

1. All the components that involve θ derivatives are zero for symmetry reasons.
2. All components that involve v_z are negligible since $v_z \ll v_\theta$
3. the two previous items together with incompressibility imply that all the components containing v_r are negligible.

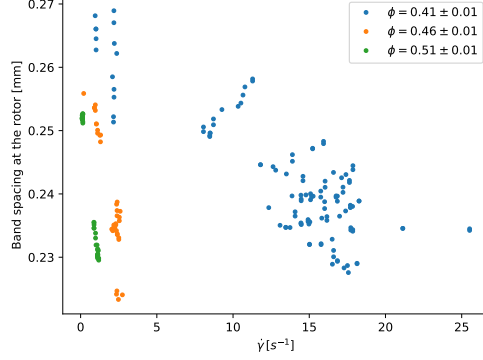


Figure 5: inter-band distance at the rotor as a function of the local shear rate.

Thus, in the computation of e_{ij} , only remain the components $r \frac{\partial(v_\theta/r)}{\partial r}$ and $\frac{\partial v_\theta}{\partial z}$. Then the invariant 2D shear rate can be written as:

$$\dot{\gamma}_{2D} = \sqrt{\left(r \frac{\partial(v_\theta/r)}{\partial r}\right)^2 + \left(\frac{\partial v_\theta}{\partial z}\right)^2} \quad (3)$$

Figure 6 shows the difference between $\dot{\gamma}_{2D}$ and $\dot{\gamma}_{1D}$ where $\dot{\gamma}_{1D} = r \frac{\partial(v_\theta/r)}{\partial r}$ is the shear rate in a 1D flow. The maximum error is around 10% which is negligible compared the other uncertainties in the results presented in the main paper.

The 2D character of the flow also influences the measurement of Σ_{33}^p that is obtained from the vertical concentration profiles and has to be taken into account in the resolution of the Cauchy equation:

$$\nabla \cdot \Sigma^p = -\Delta \rho \phi g \quad (4)$$

The z projection of this equation gives:

$$\frac{\partial \Sigma_{rz}}{\partial r} + \frac{1}{r} \left(\frac{\partial \Sigma_{\theta z}}{\partial \theta} + \Sigma_{rz} \right) + \frac{\partial \Sigma_{zz}}{\partial z} = \Delta \rho \phi g \quad (5)$$

The first two left hand terms are zero or negligible since

$$\Sigma_{rz} = \mathcal{O}(\eta_s \dot{\gamma}_{rz}) \ll \Sigma_{\theta z}$$

and

$$\frac{\partial \Sigma_{\theta z}}{\partial \theta} = 0$$

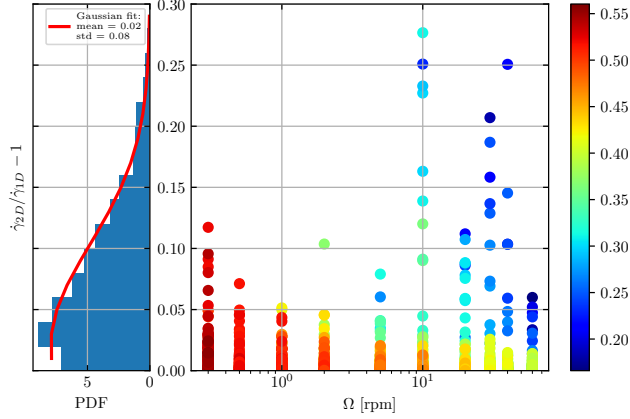


Figure 6: Ratio between the shear rate evaluated considering that the flow is 2D (3) and the shear rate calculated for a 1D flow.

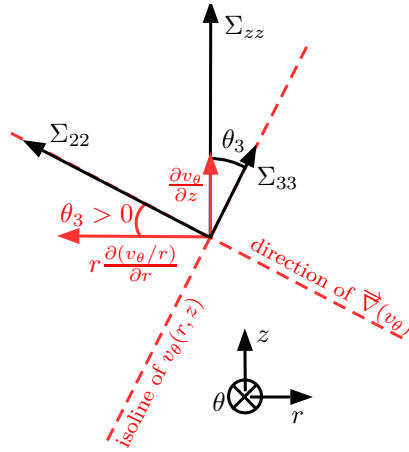


Figure 7: θ_3 is defined as the angle between the local vorticity and the vertical direction z . θ_3 is computed from the z and r derivatives of v_θ .

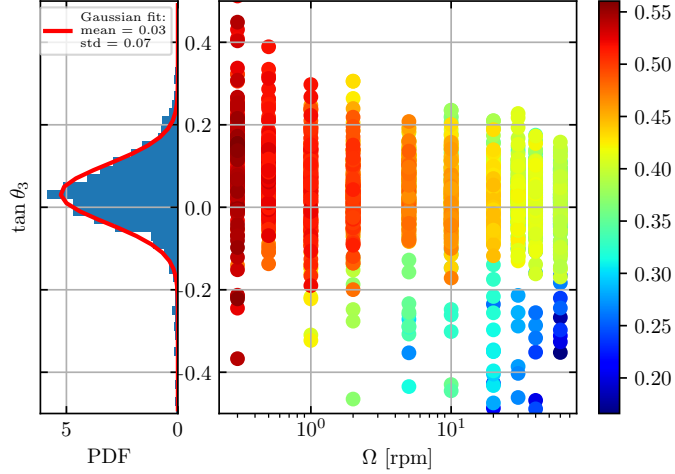


Figure 8: Tangent of the angle between the local vorticity and z . left: histogram of $\tan \theta_3$, right: variation of $\tan \theta_3$ with the angular velocity for different particle concentrations whose value is given by the color bar.

Thus, the Cauchy equation reduces to:

$$\frac{\partial \Sigma_{zz}}{\partial z} = \Delta \rho \phi g \quad (6)$$

with

$$\Sigma_{zz} = \Sigma_{33} \cos \theta_3 + \Sigma_{22} \sin \theta_3 \quad (7)$$

and (see figure 7)

$$\tan \theta_3 = -\frac{\frac{\partial v_\theta}{\partial z}}{r \frac{\partial (v_\theta/r)}{\partial r}} \quad (8)$$

Then, writing $\Sigma_{22} = \frac{\lambda_2}{\lambda_3} \Sigma_{33}$ morris1999curvilinear, we obtain the following relation between Σ_{zz} and Σ_{33} :

$$\Sigma_{33} = \frac{\sqrt{1 + \tan^2 \theta_3}}{1 + \frac{\lambda_2}{\lambda_3} \tan \theta_3} \Sigma_{zz} \quad (9)$$

with, according to morris1999curvilinear, $\lambda_2/\lambda_3 = \mathcal{O}(2)$.

Thus if the flow can be approximated by a 1D flow, $\theta_3 \approx 0$ and an estimate of the error that is made by equating Σ_{33} to Σ_{zz} can be obtained by evaluating $\tan \theta_3$ (8). In figure 8, both an histogram of the values of $\tan \theta_3$ and the variation

of $\tan \theta_3$ with Ω and ϕ are shown. It is observed in the histogram that the mean value of θ_3 is very close to zero and the variation of θ_3 with Ω and ϕ shows that, in average, θ_3 deviates from 0 only for the lowest angular velocities and the highest particle volume fractions and that, in the worst cases, $\tan \theta = \mathcal{O}(0.1)$ which according to (9) leads to an error of about 15% on Σ_{33} .

This error should be compared to the data dispersion observed for the highest particle volume fractions in figure 10 of the paper, from which it can be concluded that is negligible and that the 1D flow approximation that has been made for processing the data is relevant.

References

- [Gallier *et al.*(2016)Gallier, Lemaire, Lobry & Peters] GALLIER, STANY, LEMAIRE, ELISABETH, LOBRY, LAURENT & PETERS, FRANCOIS 2016 Effect of confinement in wall-bounded non-colloidal suspensions. *Journal of Fluid Mechanics* **799**, 100–127.
- [Jana *et al.*(1995)Jana, Kapoor & Acrivos] JANA, SC, KAPOOR, B & ACRIVOS, A 1995 Apparent wall slip velocity coefficients in concentrated suspensions of noncolloidal particles. *Journal of Rheology* **39** (6), 1123–1132.
- [Yeo & Maxey(2010)] YEO, KYONGMIN & MAXEY, MARTIN R 2010 Ordering transition of non-brownian suspensions in confined steady shear flow. *Physical Review E* **81** (5), 051502.